

Groundwater flow system analysis in the regolith of Dodowa on the Accra Plains, Ghana

Jan Willem Foppen^{a,*}, George Lutterodt^b, Gabriel C. Rau^{c,d}, Obed Minkah^a

^a IHE Delft Institute for Water Education, P.O. Box 3015, 2601 DA, Delft, The Netherlands

^b School of Engineering and Technology, Central University, Box 2305, Tema, Ghana

^c Karlsruhe Institute of Technology (KIT), Institute of Applied Geosciences, Karlsruhe, Germany

^d Connected Waters Initiative Research Centre (CWI), The University of New South Wales (UNSW), Sydney, Australia

ARTICLE INFO

Keywords:

Weathered basement
Saprolite
Local groundwater systems
Groundwater tidal analysis
Waste water infiltration

ABSTRACT

Study Region: Accra Plains. **Study Focus:** We conducted a field geology mapping, a well inventory exercise, used ERT, drilled boreholes at 8 locations (15–60 m depth), took drill core samples which we subjected to dilute acid leaching experiments, installed piezometers and equipped them with pressure transducers, analyzed tidal signals in high frequency groundwater hydrographs, carried out pumping tests, and, finally, took 49 groundwater samples. **New Insights:** Our results indicated a diverse groundwater system. On the one hand, groundwater was found at shallow depths in the saprolite of the Togo Structural Unit (TSU), which, in unweathered state, is composed of phyllites, schists, and quartzites. This system was shallow and predominantly unconfined, as revealed by tidal analysis. In addition, transmissivities of TSU saprolite, all in the order of $< 6 \times 10^{-5}$ m²/s, reduced with depth, which indicated either the lack of a stratiform fractured layer or the presence of such layer beyond drilled depths. On the other hand, groundwater was found in fractures of the gneisses of the Dahomeyan Structural Unit (DSU). This system was potentially deeper, but DSU transmissivities were significantly lower than those of TSU saprolite. Hydrochemically, groundwater was mainly characterized by infiltration of wastewater, evidenced by elevated ion concentrations, including nitrate. Due to the thinly weathered basement, groundwater system development in the area is local and restricted to the Dodowa area.

1. Introduction

Groundwater from shallow wells, boreholes and springs remains a major source of water for various uses in Sub-Saharan Africa (SSA; Howard et al., 2003; MacDonald et al., 2012; Lutterodt et al., 2018). Although a large part of SSA is covered with impervious basement rock of crystalline or metamorphic origin, the weathered upper part including fractured bedrock, usually known as basement aquifers (Wright, 1992), stores large quantities of extractable groundwater for human consumption (Foster, 1984; Wright, 1992; Lachassagne et al., 2011; Lapworth et al., 2013; MacDonald et al., 2012). Generally speaking, basement aquifers are thought to be composed of (from top to bottom) (e.g. Wyns et al., 2004; Dewandel et al., 2006; Courtois et al., 2010; Lachassagne et al., 2011; Belle et al., 2018; Alle et al., 2018): (1) an unconsolidated alterite or saprolite generally rich in clay, which comes from the advanced weathering of the parent rock (e.g. Belle et al., 2018). This layer can be subdivided into two units: alloterites, which are subject to rock volume reduction due to leaching of chemical constituents of the rock, and underlying isalterites in which the parent rock structure is

* Corresponding author.

E-mail address: j.foppen@un-ihe.org (J.W. Foppen).

<https://doi.org/10.1016/j.ejrh.2020.100663>

Received 26 February 2019; Received in revised form 12 December 2019; Accepted 3 January 2020

Available online 07 February 2020

2214-5818/ © 2020 The Authors. Published by Elsevier B.V. This is an open access article under the CC BY-NC-ND license (<http://creativecommons.org/licenses/by-nc-nd/4.0/>).

preserved with little or no volume change. In plutonic rock, the base of the isalterite very often shows a laminated layer of some 15–>30 m, which represents the highly weathered parent rock with a coarse sand-size clast texture and a millimeter-scale dense horizontal lamination cross-cutting the biggest minerals (Vassolo et al., 2019; Dewandel et al., 2006). Saprolites are not very permeable with an average hydraulic conductivity $\sim 10^{-6}$ m/s (~ 0.1 m/d), while the lower part of the saprolite is composed of a laminated layer with permeabilities 100–1000 times lower, (2) a stratiform fractured layer (SFL) characterized by a dense network of fractures in the first meters. The fracturing density and therefore the permeability of the formation, then decreases with depth (Maréchal et al., 2004; Dewandel et al., 2006; Lachassagne et al., 2014; Belle et al., 2018). The SFL is anisotropic and has a transmissive function within the overall composite aquifer (SFL + saprolite) (Belle et al., 2018), (3) unweathered bedrock, which can be regarded impervious and as having very low storativity (Maréchal et al., 2004). This conceptual model of paleo weathering profiles on hard rock, as described above applies to basement rock of crystalline or metamorphic origin (e.g. gneiss). Also in case of schists or a more diverse geology composed of combinations of shales, phyllites, schists and quartzites, in a tropical environment such weathering profile seems to exist: Tsozué and Yongue-Fouateu (2017) describe a 10 m thick weathering profile of a garnet rich micaschist in the rainforest zone of Cameroon, which is composed of (from bottom to top) a coarse saprolite, a fine saprolite with many isalteritic relicts, and a set of clayey horizons, with at its base nodules with a fine blocky structure. Vassolo et al. (2019) distinguished four weathering zones with total thicknesses up to 80 m in a geologically diverse schist-shale-quartzite environment in their study area in tropical Burundi composed of (from bottom to top) a fractured layer or saprock (their deeper aquifer), isalterite, alloterite, and a collapsed clay rich plasmic zone, only in valleys. The isalterites were made up by coarse sand to fine gravel, sandy shales, alternations of shales and quartzites, reddish silty clay, or clayey schists with layers of non-swelling red clay, while the alloterites were composed of clays, weathered schists, or sandy schists (Vassolo et al., 2019).

Wright (1992) notes that transmissivities of basement aquifers in SSA are usually in the range of 1.2–3.5e-5 m²/s, which yields sufficient water for small scale use but do not allow large scale groundwater development. Edet and Okereke (2005) found transmissivities in the order of 5.8e-6 m²/s, while in southern India, Guihéneuf et al. (2014) obtained values of 0.7–4.6e-4 m²/s, which are all in the same range as reported by Wright (1992).

The objective of our study is to characterize the shallow hydrogeological system in the weathered basement rock dominated Dodowa area in terms of aquifer types, water quantity and quality in order to underpin the preparation of a groundwater management plan.

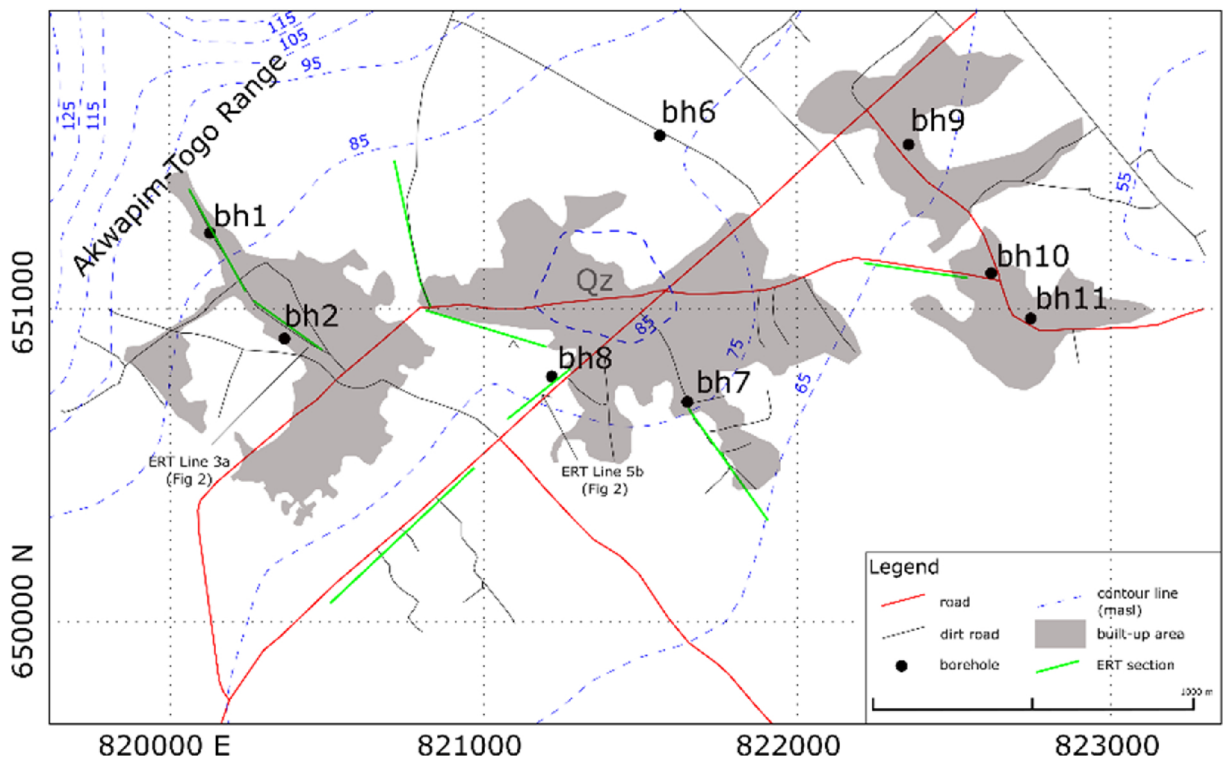
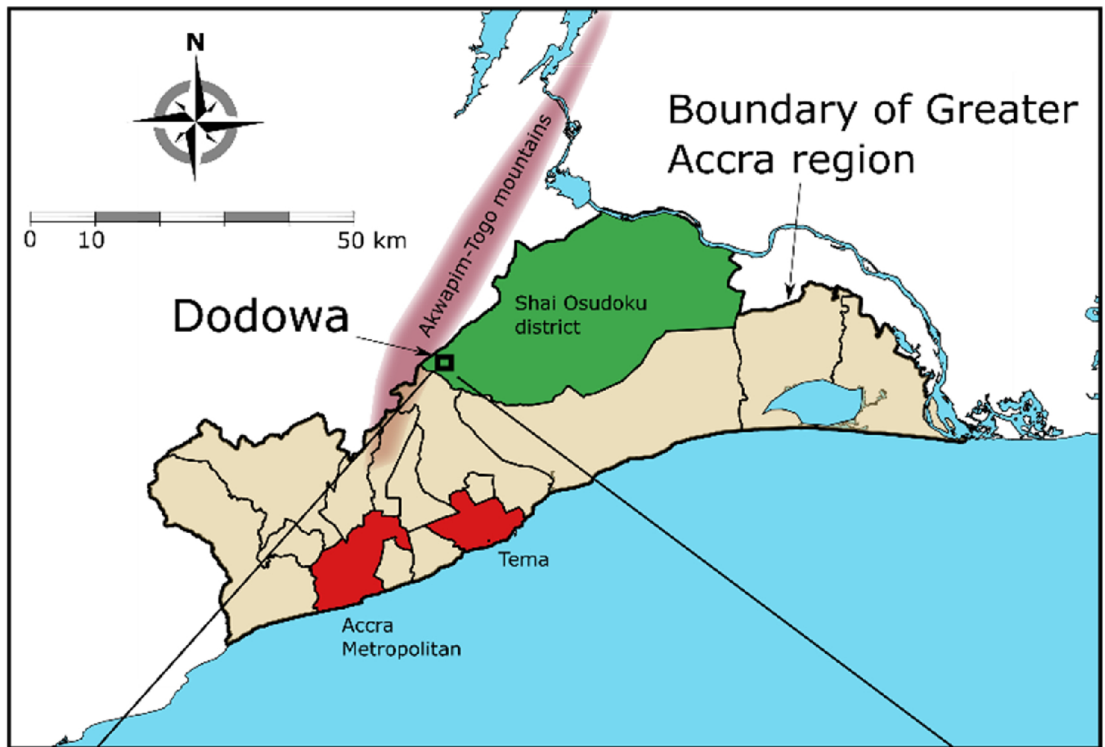
2. The DODOWA study area

Dodowa is located in the Shai Osudoku district in the south eastern part of the Greater Accra Region, Ghana (Fig. 1), close to the Akwapim-Togo mountain range. The district receives a mean annual rainfall of about 900 mm per year, and with an average temperature of 27 °C (Kortatsi and Jørgensen, 2001), the climate can be considered tropical (Kabo-Bah et al., 2016). The region experiences two rain seasons occurring between May and July and between September and October (Kortatsi and Jørgensen, 2001). Vegetation in the area is mainly forest on the hills, and grassland with mango trees interspersed with small agricultural plots in the lower parts. Topographically, the northwestern part of Dodowa is hilly with elevations of 125–150 m.a.s.l., while the eastern and southern part have an almost flat topography with elevations of 55–65 m.a.s.l. The geology of the area is mainly composed of the Togo Structural Unit (TSU) and Dahomeyan Structural Unit (DSU). The TSU comprises a series of metamorphic and highly folded quartzites, phyllites and schists. Ar⁴⁰/Ar³⁹ (muscovites) dating showed that the TSU is 579.4 ± 0.8 Ma in age (Attoh et al., 1997; Neo Proterozoic). By means of a major thrust fault, the TSU covers sequences of the DSU, which is also older, still Neo Proterozoic, and mainly found in the low-lying plains (Attoh et al., 1997). The DSU has experienced metamorphism and the unit occurs as alternate belts of acid and basic gneisses. Here and there the low-lying gneissic plain is occupied by isolated inselbergs and ridges of ultrabasic intrusive as well as hills forming outliers of the TSU (Attoh et al., 1997). In the study area both the TSU and DSU have undergone intense weathering, which resulted in an unconsolidated top-layer or regolith with groundwater tables within 5 m below the land surface. With a population of about 15,000 in Dodowa, most inhabitants are engaged in agriculture. Households use water from a variety of sources. For ~ 38 % of the population, the main source is groundwater from privately dug wells or boreholes, while 56 % have access to piped water from the public water supplier (Grönwall, 2016). Except for a main source, the majority (55 %) of the population also reported having a second water source, which functions as a back-up. Of those having a second source, 73 % uses groundwater from dug wells or boreholes.

3. Materials and methods

3.1. Electrical resistivity tomography (ERT)

To determine geological structures and groundwater potential of the study area, ERT was carried out in 7 sections with a total length of 3200 m and a maximum depth of 60 m by employing an ABEM Terrameter SAS 1000 resistivity meter in multi-electrode set-up. This technique runs both profiling and vertical electrical sounding concurrently continuous vertical electrical soundings [CVES] to produce a two-dimensional 2D resistivity pseudo-section output of the subsurface with spatial resolution of 5 m. A quality check of the data was carried out, and bad data points were removed before inverting the data with the RES2DINV modelling software (Loke and Barker, 1996). Final output from RES2DINV used in this study were modelled apparent resistivity sections.



(caption on next page)

Fig. 1. The Dodowa study area is located in the south eastern Shai Osudoku district within the Greater Accra region (upper map). The study area (lower map) is around 6 km² and includes the built-up areas of Dodowa, the area immediately south of these built-up areas and also branches of the Akwapim-Togo mountain range, which itself is located just north of the study area. The map of the study area includes locations of ERT sections and boreholes.

3.2. Borehole drilling, drill core sampling, and piezometer installation

At 8 locations throughout the Dodowa area 6 inch diameter boreholes with depths ranging from 15 to 60 m were drilled using a MAN DIESEL Speed Star drilling rig fitted with 300 psi compressor in rotation with direct circulation whereby rock destruction was achieved by using air or water. When required, drilling was carried out by a drag bit in roto-percussion mode with a Down-The-Hole hammer. Every meter, drill cuttings were collected and the lithology was visually observed, described and recorded. Drill cuttings were taken to the IHE Delft analytical laboratory, Delft, The Netherlands, for further analysis (see below). The general lay-out of each borehole is depicted in Fig. 2. In two boreholes (BH2 and BH10) at 5 m depth 2 inch pipes were fitted to the sides of the 4 inch diameter PVC in order to obtain groundwater table observations at shallow depth. The constructed boreholes were developed by both air lift and surging until the discharging water was clear. Finally, each borehole was covered by a concrete slab, a (locked) cage, and a (locked) lid in order to prevent people from starting to abstract groundwater from the piezometer and/or to prevent contamination of groundwater from above (Fig. 3).

3.3. Reconnaissance survey of exposed rocks and well inventory

A number of reconnaissance walks were carried out to make an inventory of existing large diameter (1 – 2 m) dug wells and to identify exposed geological formations in the Dodowa area. In addition, of 30 dug wells, selected based on accessibility, while making sure the selected wells were evenly spread over the area, elevations relative to mean sea level were determined using a Topcon DT-20B digital theodolite.

3.4. Groundwater level observations

A number of newly installed piezometers were equipped with pressure transducers (Mini-Diver DI501; Schlumberger) to record pressure at 20 min intervals. The barometric pressure was measured in a well-attended place inside a compound within the center of Dodowa using a barometric diver (Mini-Diver DI500; Schlumberger) in order to correct pressures recorded in the well for atmospheric pressure. In addition, for the 30 leveled large diameter dug wells with a measuring tape groundwater levels were recorded every 2 weeks from early 2016 to mid-2017.

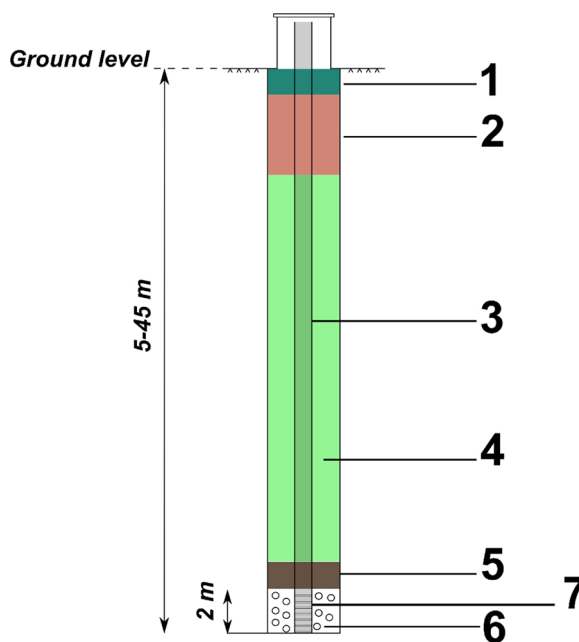


Fig. 2. Design of each 4 inch piezometer. 1: Cement grouting, 2: clay sealing, 3: 4 inch PVC pipe, 4: backfill material, 5: cement/sand mixture, 6: 4 – 8 mm natural gravel packing, 7: slotted screen.



Fig. 3. BH8 – 50 m (foreground), BH8 – 35 m, BH8 – 24 m, and BH8 – 15 m (background). The horizontal distance between each borehole is 4 – 7 m. Each borehole is covered by a concrete slab, a (locked) cage, and a (locked) lid in order to prevent abstraction and contamination.

3.5. Groundwater tidal analysis

The groundwater response to Earth and atmospheric tides can be used to detect confinement and, if confined, calculate the barometric efficiency (BE) (Acworth et al., 2016; McMillan et al., 2019). We refer to this as tidal analysis from here onward and note that this is not associated with ocean tides. The presence of an Earth tide M_2 (at a frequency of 1.93227 cycles per day (cpd)) amplitude that is significantly stronger than the background noise indicates confined conditions, whereby the magnitude is proportional to the degree of confinement (Rahi and Hallihan, 2013). Under unconfined conditions the M_2 amplitude is absent but the presence of an atmospheric tide S_2 (at a frequency of 2 cpd) amplitude indicates a delay in atmospheric pressure transfer through the vadose zone caused by a delay in response to barometric forces acting on the pore pressure in the subsurface and the measured water level in the piezometer (Rasmussen and Crawford, 1997). This time lag indicates a lower pneumatic permeability of the vadose zone (compared to an instantaneous response), semi-confined conditions and therefore also decreased vulnerability to groundwater contamination from the surface (Hussein et al., 2013). The presence of both M_2 and S_2 amplitudes indicates confined conditions and justifies the calculation of BE as well as specific storage and compressibility (Acworth et al., 2015, 2016; Rau et al., 2018).

In this study, recorded groundwater levels and atmospheric pressure were used to determine the degree of confinement and BE using a new combination of the approaches explained in the works of Rahi and Hallihan (2013) and Acworth et al. (2015, 2016, 2017). We quantified amplitudes and phases of M_2 and S_2 for atmospheric (depicted as superscript AT) and groundwater (depicted as superscript GW) pressure (measured) and Earth tide (synthesized, depicted as superscript ET) records using the Fast Fourier Transform (FFT) implemented in the *python* programming language. Earth tides for Dodowa (Latitude: 5° 52.902' N, Longitude: 0° 5.835' W, Height: 88 m.a.s.l., period October 2016-July 2017) were calculated using the PyGTide toolbox (Rau, 2018). For confined conditions, BE was further calculated as (Acworth et al., 2016):

$$BE = \frac{S_2^{GW} + S_2^{ET} \cos(\Delta\phi) \frac{M_2^{GW}}{M_2^{ET}}}{S_2^{AT}} \quad (1)$$

where S_2^{GW} is the amplitude of the groundwater level, S_2^{ET} is the amplitude of the Earth tide and S_2^{AT} is the amplitude of the atmospheric tide (all at 2 cpd frequency); M_2^{GW} is the amplitude of the groundwater level and M_2^{ET} is the amplitude of the Earth tide (both at 1.9324 cpd frequency). Using a realistic range of assumed subsurface porosity θ [-] values, the formation compressibility (Pa^{-1}) and specific storage were calculated using (Jacob, 1940)

$$\alpha = \frac{\theta\beta(1 - BE)}{BE} \quad (2)$$

and

$$S_s = \rho g(\alpha + \theta\beta) \quad (3)$$

where β is the water compressibility (Pa^{-1} ; $4.59 \times 10^{-10} \text{ Pa}^{-1}$ at 20 °C). Results from this method are more accurate compared to time domain approaches (Turnadge et al., 2019).

3.6. Pumping tests

In the newly installed piezometers (described above) pumping tests and a series of slug tests were carried out to determine transmissivity and hydraulic conductivity of the aquifer. Pumping tests involved continuously pumping (discharging) a borehole at a constant rate until the water level dropped to the depth of the pump (around 3 m above the bottom of the borehole). The duration of the tests varied between 30 – 360 min. After pumping, water levels were recorded until recovery to the initial water level. These recovery tests took 55 – 180 min.

BH8 consists of 4 separate boreholes at various depths (15, 25, 35, and 50 m; Fig. 3). During the pumping test in one BH8 hole, groundwater levels in other BH8 holes were observed. In this way, hydraulic conditions and the connectivity between the various

screens at BH8 could be determined. Slug tests were carried out for 2 inch diameter piezometers and for piezometers in low permeability layers. Thereto, one or more bails of known volume were taken out of the piezometer and groundwater level recovery was determined using a measuring tape. Data from all tests were analyzed using the software package MLU (Hemker, 1999), which is based on a 3D analytical solution for transient well flow in layered aquifer systems, whereby transmissivities and resistance values of the hydraulic system are determined via curve fitting. Resistance in this case is defined by the quotient of the saturated thickness and vertical hydraulic conductivity, usually of an aquitard. When expressing the saturated thickness in m and the hydraulic conductivity in m/s, then the resistance is expressed in s. Unlike other aquifer test analysis software supporting a wide variety of different solution types for one and sometimes two aquifers (e.g., Theis, Hantush, Neuman, Boulton, Papadopoulos, Moench, Bouwer-Rice), MLU is based on a single analytical solution technique for well flow that handles multi-aquifer systems (aquifers and aquitards), single layered (stratified) aquifers, unconfined, confined, leaky, and delayed yield aquifer conditions, effects of aquifer and aquitard storativities, wellbore storage and skin effect for each pumping well and observation well, and partial penetration (Hemker, 1999; Carlson and Randall, 2012).

3.7. Groundwater sampling

49 Fresh groundwater samples were collected in clean 250 ml polyethylene bottles. Immediately after sampling, EC, temperature and pH were measured with handheld meters (Greisinger GMH3431 and GMH3530 including a GE100BNC pH electrode). Then, samples were stored in a cool box or refrigerator, and alkalinity was determined by titrating with 0.2 M sulphuric acid using a portable titration set in a temporary laboratory in the center of Dodowa within 24 h after sample taking. With a HACH DR 900 colorimeter, nitrate was determined using the cadmium reduction method #8039, sulphate using the SulfaVer method #8051, phosphate using the ascorbic acid method #8048, silica using the silicomolybdate method #8185, and ammonium using the salicylate method #10,031.

Samples for cations (K, Mg, Ca, Mg, Fe and Mn) and anions (Cl and SO₄) were filtered through a 0.45 µm cellulose acetate filter into 25 ml scintillation vials. Cation samples were further preserved by adding two drops of concentrated nitric acid. Total Organic Carbon (TOC) samples were prepared by adding 2 drops of concentrated sulphuric acid. Then, the samples were frozen. After collection, all samples were shipped to the IHE Delft analytical laboratory to determine cations using an ICP-MS (Thermoscientific, Xseries 2), anions by Ion Chromatography (IC - Dionex ICS-1000), and TOC using a Shimadzu Total Organic Carbon Analyzer TOC-L series. With the results of the analyses, speciation calculations were carried out using PHREEQC (Parkhurst and Appelo, 1999), but only for those samples with a charge balance error within ±15 %. Samples with ion balance errors in excess of ±15 % were discarded.

3.8. Reactive metal ions

In order to obtain an indication of the geo-available or extractable metal ions and to assist in identifying the hydrochemical signature of groundwater in the aquifers in unpolluted condition, we employed the dilute nitric acid method (ISO-17586:2016). Thereto, after drying and sieving, 0.2 g of sieved (2 mm) drill cuttings was mixed with 2 ml of 0.43 M nitric acid, and then mixed for 24 h. Mixing was carried out in centrifuge tubes standing up straight using an orbital shaker at 150 rpm. After mixing, 10 ml of demineralized water was added, and samples were centrifuged for 10 min at 4500 rpm. Supernatants were measured on an ICP-MS as described above.

4. Results

4.1. Geology of the area

We found that the boundary of TSU and DSU was exposed and could be easily mapped in the central built-up area of Dodowa (Fig. 4), where both quartzite belonging to TSU and gneiss belonging to DSU were exposed. In addition, we observed a layer of conglomerates, including the presence of angular breccia-type fragments in the vicinity of old Ghanata high school to the highest parts of Dodowa, in the so-called Zongo area, also located in the central built-up area. ERT results showed that apparent resistivities ranged from more than 500 to less than 1 Ωm (Fig. 5). For the TSU, composed of phyllites, schists, and quartzites, including its weathering products, we attributed < 10 Ωm to clay, 10–200 Ωm to sandy clay with quartzite rock fragments, and > 250 Ωm (up to several 1000 Ωm) to quartzite. Furthermore, the conglomerate had an apparent resistivity > 200 Ωm (up to 600 Ωm; Fig. 5, line 3a), and for the gneisses of the DSU, resistivity values > 200 Ωm (up to several 1000 Ωm) were attributed to parent gneiss, while values < 200 Ωm were attributed to saprolite above the gneiss. Generally speaking, the thickness of the saprolite of the TSU ranged from 0 m at BH7 to more than 50 m towards the hilly northwest of Dodowa (Fig. 4). The presence of the TSU saprolite was confirmed by the drillings and was mainly composed of (lateritic) clays and sandy clay. Since thickness, geology and resistivity values of TSU saprolite ranged considerably, we inferred that the parent TSU must have been diverse as well, and likely composed of softer and more weatherable phyllites and schists, intercalated with less weatherable quartzitic layers. At BH8 and BH1, we drilled up to such less weatherable, parent, quartzite. In contrast to the TSU, the thickness of the DSU saprolite was less than 10 m (BH9, BH10, and BH11). Drilling B2 was mainly in a thick layer of conglomerate (> 15 m), which appeared to be the extension of similar material found exposed at the surface between Ghanata High School and the Zongo area (as described above).

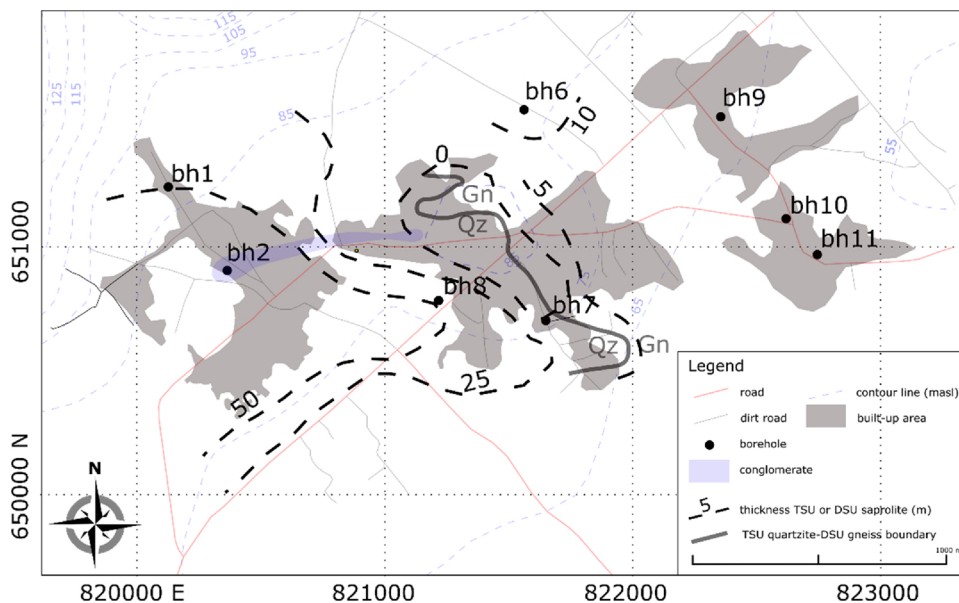
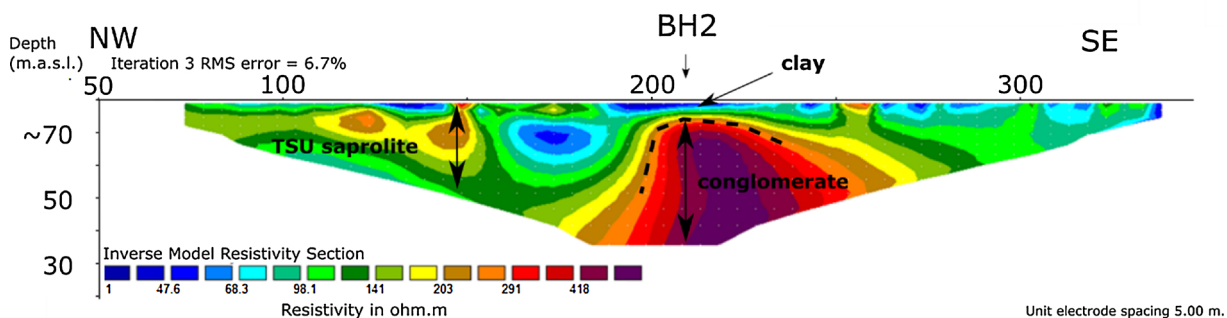


Fig. 4. Boundary between TSU and DSU, mapped based on the appearance of quartzite (TSU) and gneiss (DSU). In addition, the thickness of the saprolite (m) is indicated.

Line 3a



Line 5b

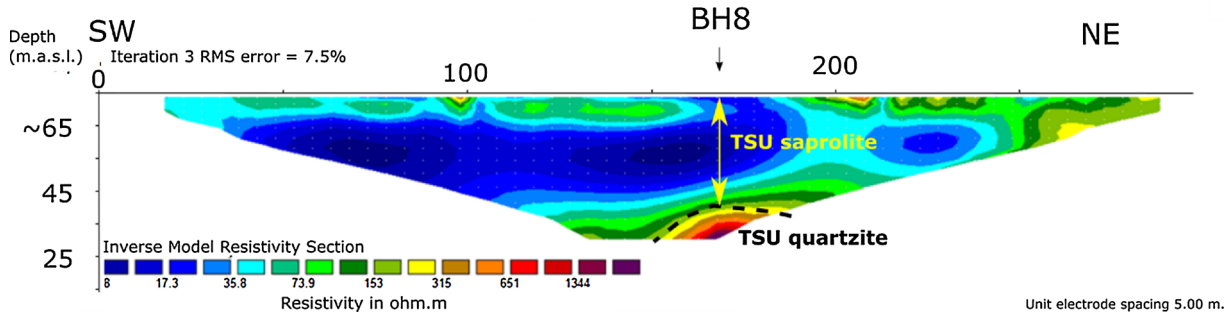


Fig. 5. Two ERT profiles depicting saprolite (low apparent resistivities), TSU SFL (high apparent resistivities), and conglomerate. The locations of sections are given in Fig. 1. A more detailed description of the weathered profile is given in the text.

4.2. Groundwater presence, groundwater levels and fluctuations

Within the TSU saprolite and the conglomerates, groundwater tables were 1–5 m below the surface. In DSU area, at some locations (e.g. BH6, BH10), groundwater was found in the DSU saprolite, while at other locations (BH9, BH11), the saprolite was dry.

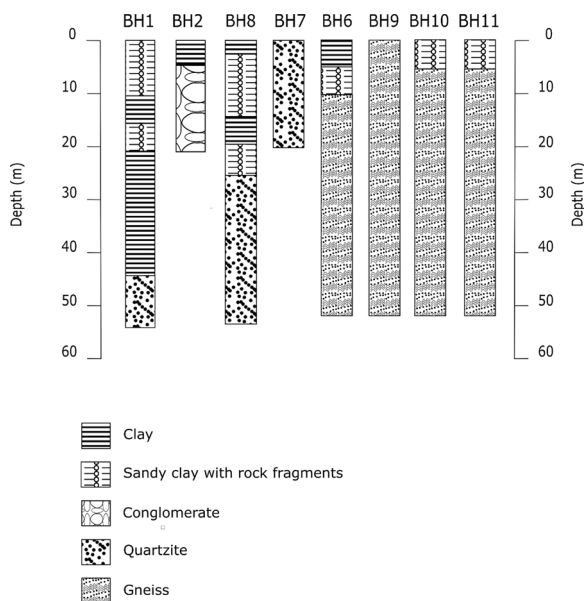


Fig. 6. Summarizing stratigraphic columns of the borehole drill cuttings carried out in the study area. Each borehole –except BH7, which was dry- is cased throughout, and has a 2 m screen at the bottom (see Fig. 2). BH8 consists of 4 boreholes drilled at 4–7 m distance from each other to 15, 24, 35, and 50 m depth, also with a 2 m screen at the bottom of each hole (see Fig. 3).

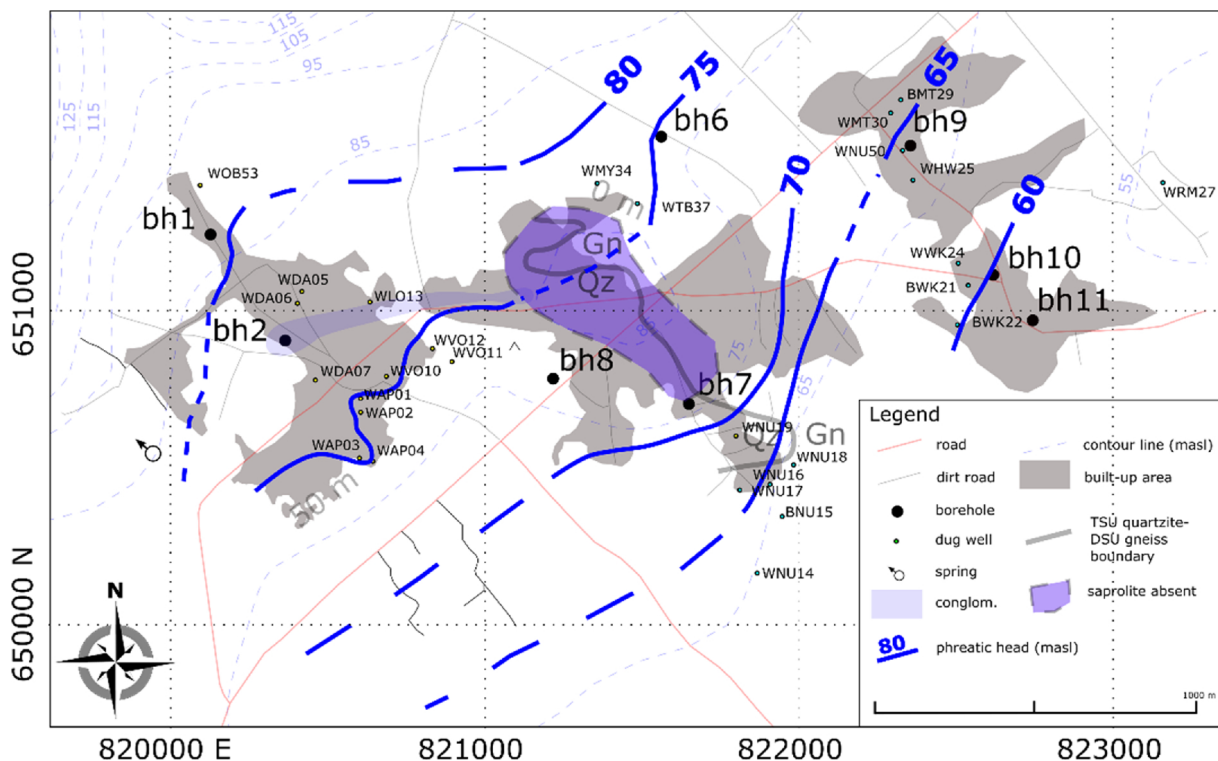


Fig. 7. Composite groundwater level map based on groundwater levels measured in dug wells and drilled wells in both TSU and DSU saprolite and DSU gneiss. Question marks indicate the uncertainty with regard to the extension of conglomerate towards the observed spring area.

This shallow groundwater, however, was perched, as the borehole became unsaturated when drilling continued. Occasionally and only in DSU gneiss, a sudden drop of the drilling bit could initiate the first appearance of water in the borehole, which indicated the presence of permeable, water-filled fractures in the DSU gneisses. For those boreholes (BH6, BH9, BH10 and BH11), we observed 1–3

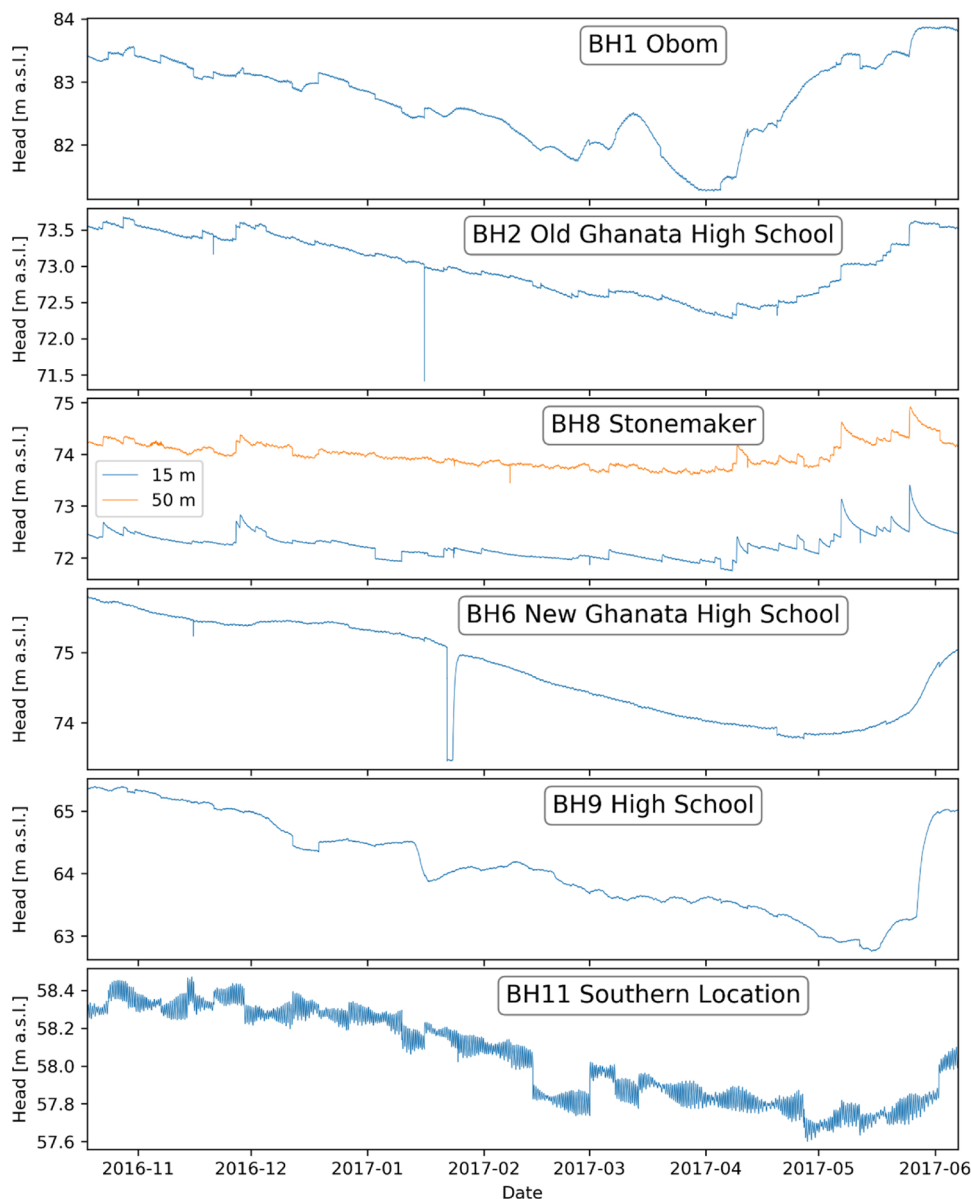


Fig. 8. Groundwater hydrographs measured at 20 min intervals.

of those drilling bit drops per borehole, indicating the presence of 1–3 water bearing fractures per ~50 m of DSU.

For the entire area, TSU, DSU, and conglomerates, we constructed a combined groundwater/piezometric level map (Fig. 7). The horizontal groundwater head gradient in the study area was from NW to SE. In all hydrographs (Fig. 8), groundwater levels gradually dropped to their lowest levels around March–May and then increased from March/May to June to reach the approximate same level as during the start-up of the level measurements in October. Recorded year-round water level fluctuations (in any year: maximum minus minimum groundwater level) in any monitored piezometer were between 1–2 m. At BH1, superimposed on the above-mentioned seasonal pattern, modest 10–20 cm almost instantaneous level increases and decreases can be seen, which we interpreted as groundwater level changes possibly due to abstraction in the vicinity of the piezometer. The characteristic groundwater level decline after a recharge event, representing the emptying of a type linear reservoir, was absent. Of all hydrographs, at BH8, those characteristic almost instantaneous increases and recession due to direct recharge and emptying of the groundwater aquifer were clearly present.

Furthermore, we observed that the head at BH8–50 m was 1–2 m higher than the head at BH8–15 m, which indicated the presence of a vertical upward gradient throughout the year. In BH11, there is a clear presence of Earth tide effects (see next paragraph), while in BH9, located close to BH11, this Earth tide effect was already completely absent.

Finally, in the groundwater hydrographs of BH2, BH8–50 m and BH6, there are brief lows in the groundwater head. This is due

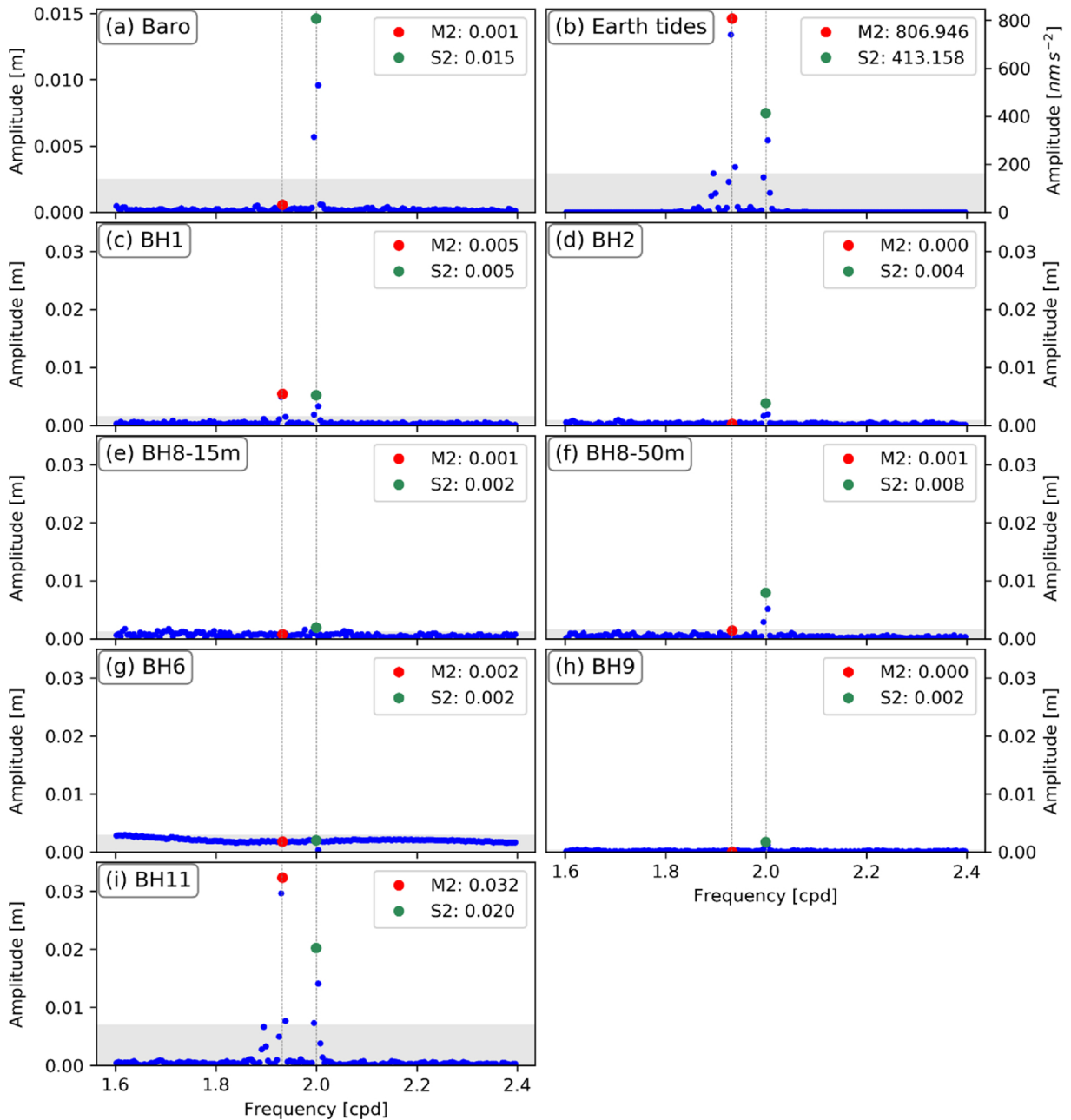


Fig. 9. Amplitude frequency plots of high resolution groundwater hydrographs. Phases at M2 and S2 frequencies are indicated in red and green; M2 and S2 values are given in the upper right of each plot and are explained in the text. (For interpretation of the references to colour in this figure legend, the reader is referred to the web version of this article).

to temporary abstractions conducted to clean the piezometers. Towards the west part of the area, groundwater heads were very shallow, and at one location, we observed a spring (Fig. 7) with a discharge in the order of 20–30 l/s (visually determined during fieldwork in October, after a rain season, when spring discharge was likely high). The discharged spring water joins the Dodowa river immediately south of Dodowa and continues to flow towards the south. From the groundwater level pattern, we concluded that the spring is likely fed by the (fractured?) quartzites towards the NW of the spring.

4.3. Groundwater tidal analysis

The groundwater level amplitude spectra limited to the frequency range of interest (range between 1.6 and 2.4 cpd) for barometric pressure, the Earth tide record and all boreholes (same vertical scale for comparison) are summarized in Fig. 9. The amplitudes

for the Earth tide component M_2 (1.93227 cpd) and the combined Earth/atmospheric tide component S_2 (2 cpd) were quantified and highlighted in the plots (red and green colored dots, respectively). Fig. 9a demonstrates the presence of atmospheric tides at 2 cpd with 1.5 cm head equivalent, whereas Fig. 9b shows the presence of both M_2 and S_2 as miniscule gravity fluctuations.

The lack of a groundwater response to Earth and atmospheric tides for BH6 and BH8 – 15 m indicated completely unconfined conditions. BH9, BH2, and BH8 – 50 m showed semi-confined conditions with an increasing S_2 magnitude indicative of a decrease in the pneumatic permeability of the vadose zone. The tidal results also illustrated that the thin clay layers found in the lithological profiles of BH2, BH8 and BH6 (Fig. 6) must have more permeable zones or be of limited horizontal extent. This is because atmospheric pressure variations can reach the point of measurement rapid enough to avoid delays which would otherwise occur when propagating through clays that are considered pneumatically tight.

BH1 and BH11 were confined as indicated by the presence of both M_2 and S_2 components. Calculated BE values for BH1 and BH11 were 0.29 and 0.99, respectively. Assuming porosities in the range of 0.5–5%, the aquifer compressibilities for the (semi-)confined cases ranged from 10^{-10} to 10^{-14} Pa⁻¹, while corresponding specific storage values ranged between 10^{-6} and 10^{-8} m⁻¹ (Table 1). From the tidal analysis we derived that most of the study area was unconfined. Towards the southern part of Dodowa, the gneiss area was (semi-)confined with a high barometric efficiency. Furthermore, the deeper part of the quartzite area in the north part of Dodowa was (semi-)confined.

4.4. Pumping tests and slug tests

Based on the results of the groundwater tidal analysis, we kept the specific storage values for the confined parts of the models we applied to the pumping and slug test data in MLU at 10^{-7} m⁻¹. In all cases only aquifer parameters were optimized; well diameter parameters were not optimized. The results indicated that transmissivities for TSU ranged from 0.5 to 5.4e-5 m²/s (Table 1). Transmissivities of 3–5.4e-5 m²/s at shallow depth (BH8 – 15 m, BH8 – 24 m) were significantly higher than 0.8–2.1e-5 m²/s at 35 – 50 m. The specific yield was highest shallow (11 % at 15 m) and lowest (2 %) deep (Table 1). From the permeability and porosity values, we inferred that we had stopped drilling in less permeable quartzite. Also, we inferred that either we had not drilled up to the more permeable stratiform fracture layer (SFL) or the SFL was not present in the case of BH1 and BH8. As an example of the goodness of fit, in Fig. 10 for one pumping test, the drawdowns for the 4 screens at various depths were given including the fitted curves. For the conglomerate, transmissivity was 3.7e-5 m²/s. Finally, for the gneiss of the DSU, transmissivities of the water bearing fractures were relatively low: 0.2–1.5e-6 m²/s.

4.5. Hydrochemistry and geochemistry

Electrical conductivity values ranged from 200–5,600 μ S/cm (Table 2), while nitrate concentrations ranged from 0–4 mmol/L (0–240 mg/L). Samples with high EC-values and no nitrate were found towards the south and south east. Due to the higher reactive metal ion concentrations, as indicated by the dilute nitric acid leaching experiments (Fig. 11), groundwater in the gneissic Dahomeyan Structural Unit contained more reactive metal ions, like calcium, sodium, and magnesium, while groundwater in the TSU was generally poor on reactive metal ions after the dilute nitric acid experiments.

In the TSU area, at the foot of the hills in the NW, EC of shallow groundwater was 207 μ S/cm (Fig. 12a), while concentrations of most ions were low, and pH was circumneutral (7.4). Groundwater here is of the NaCl and NaHCO₃ type (Table 2), mainly as a result of prolonged dissolution of silicate minerals. When going to the center of the cross-section, where there is built-up area, EC-values increase to over 3000 μ S/cm, while pH values drop 1–2 units to 5.5–6.5 (Fig. 12b). Also, alkalinity values increase from less than 0.5 mmol/L to more than 1.0 mmol/L in the center parts of the study area (Fig. 12c). Furthermore, while nitrate is absent at the fringes of the study area, towards the center, values increase to over 1.0 mmol/L (Fig. 12d). Because of the presence of nitrate in the discharging groundwater from the spring, we discarded the possibility that the watershed was located NW of the spring. For the entire study area, TOC values were generally low (<0.5 mmol C; Table 2) without clear trend. Also, in all cases, ammonium was low or absent. At the southern boundary of the study area, an increase in EC, pH, and alkalinity occurred, while nitrate values reduced to zero.

5. Synthesis, discussion and conclusions

Using our multi-parameter dataset, a rather diverse pattern of groundwater system dynamics emerges in the Dodowa area in which a number of hydrochemical processes take place. Our results indicate weathered material on top of TSU and DSU. For the TSU, composed of phyllites, schists, and quartzites, including its weathering products, we attributed < 10 O m to clay, 10–200 ohm m to sandy clay with quartzite rock fragments, and > 250 O m (up to several 1000 O m) to quartzite. Furthermore, the conglomerate had an apparent resistivity > 200 O m (up to 600 O m), and for the gneisses of the DSU, resistivity values > 200 O m (up to several 1000 O m) were attributed to parent gneiss, while values < 200 O m were attributed to saprolite above the gneiss. Generally speaking, the thickness of the saprolite of the TSU ranged from 0 m at BH7 to more than 50 m towards the hilly northwest of Dodowa (Fig. 4). The presence of the TSU saprolite was confirmed by the drillings and was mainly composed of (lateritic) clays and sandy clay. Saprolite thicknesses varied considerably: in the center of Dodowa, saprolite is absent and here, quartzitic TSU besides gneissic DSU is exposed at the surface. Towards the west, TSU saprolite thickness is more than 50 m, and to the south 25 m or less, while the DSU saprolite thickness is less than 10 m. Since thickness, geology and resistivity values of TSU saprolite ranged considerably, we inferred that the parent TSU must have been diverse as well, and likely composed of softer and more weatherable phyllites and schists, intercalated

Table 1
Results of the tidal analysis (upper part) and the pump/slug tests (lower part). The degree of confinement was determined from measured high resolution groundwater hydrographs and so were aquifer compressibilities and specific storage values for (semi-)confined locations BH1 and BH11. From the degree of confinement analysis conditions for the pump and slug tests were obtained.

Well or piezometer	BH1-4"	BH2-4"	BH8 - 15 m	BH8 - 24 m	BH8 - 35 m	BH8 - 50 m	BH6-4"	BH6-2"	BH9	BH10-2"	BH10-4"	BH11
Tidal analysis*												
Rock type	TSU	Conglomerate	TSU	TSU	TSU	TSU	DSU	DSU	DSU	DSU	DSU	DSU
M2	0.005	0.000	0.001			0.001	0.002	0.000	0.000			0.032
S2	0.005	0.004	0.002			0.008	0.002	0.002	0.002			0.020
Degree of confinement	leaky	unconf.	unconf.			unconf.	unconf.	unconf.	unconf.			confined
BE	0.293											0.993
Porosity range	0.005-											0.005-0.05
α range	0.05											1.7e-14 -
	5.5e-12 -	5.55e-11										1.7e-13
S_s range	7.7e-8 -											2.3e-8 -
	7.7e-7											2.3e-7
Pump- or slug test												
Test performed	Pump	Pump	Pump	Pump	Pump	Pump	Slug	Slug	no test	Slug	Slug	no test
Observations wells	well itself	well itself	BH8-24 BH8-35 BH8-50	BH8-15 BH8-35 BH8-50	BH8-15 BH8-24 BH8-50	BH8-15 BH8-24 BH8-35	well itself	well itself	no test	well itself	well itself	
Analysis conditions	leaky	unconfined	unconfined	unconfined	unconfined	unconfined	unconfined	unconfined		unconfined	unconfined	
Transmissivity (m2/s)	4.40E-06 (12 %)**	3.66E-05 (3 %)	3.65E-05 (15 %)	5.38E-05 (16 %)	2.13E-05 (13 %)	1.52E-05 (20 %)	1.50E-06 (11 %)	4.63E-07 (14 %)		2.31E-07 (2 %)	1.04E-06 (17 %)	
Resistance (s)	8.80E-06 (12 %)		0.11 (10 %)	0.08 (15 %)	0.03 (21 %)	0.02 (23 %)						
Storage coefficient (c)	0.46	0.04	3.51	12.01	11.66	12.11	0.03	0.12	0.00	0.03		
Sum of squared residuals (m²)												
Pump/slug regime (m³/s)	4.5E-04 / 1.9E-04	3.0E-04 / 6.8E-04	2.15E-04	3.17E-04	2.66E-04	1.67E-04	2.50E-04	1.67E-04	8.33E-05	2.50E-04		
Duration pump or slug regime (s)	2700 / 12000	2100 / 21600	21600	18000	21600	21600	300	30	60	300		

*: Baro: M2 = 0.001; S2 = 0.150; Earth tides: M2 = 806.946; S2 = 413.158.

** : Values in parentheses are standard deviations expressed as a percentage of the estimated value.

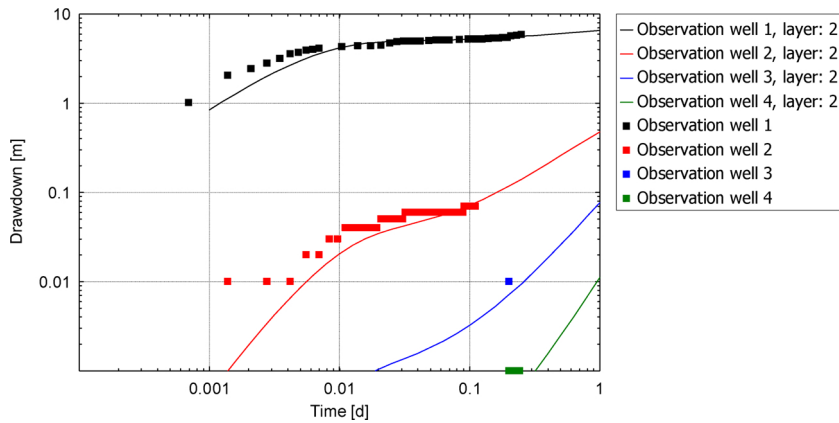


Fig. 10. Example of measured pumping test data (squares) and MLU fit (line) for piezometer BH-15 m in case of unconfined conditions (logarithmic curve fitting in MLU).

with less weatherable quartzitic layers. Quist (1976), as reported in Kortatsi (2006), mentioned similar thicknesses of weathering depths of the TSU: 47 m near the foothills of the Akwapim-Togo range, and decreasing to less than 6 m in the heart of the Accra Plains, south of the study area.

In the TSU, groundwater occurrence was mainly in the saprolite, while in the DSU, groundwater occurrence was mainly in a limited number of water transmitting fractures (around 3 fractures per 50 m DSU). Results from groundwater tidal analysis illustrated that most of the study area can be considered unconfined, while the northern TSU saprolite (BH1) and the southern fractured gneiss of DSU (BH11) form a (semi-)confined aquifer. From this it is clear that the clay layer in the vicinity of BH8 above BH8-35 and BH8-50 does not give rise to confinement, as both high frequency groundwater level series we measured in BH8 boreholes are unconfined. The clay layer in BH1, which had a larger thickness than at BH8, was apparently capable of partly confining groundwater. Transmissivities of the TSU saprolite ranged from 0.5 to 5.4e-5 m²/s and increased from bottom to top. These values are less than the 5.6e-5-1.1e-3 m²/s given by WRRRI (1996), as reported by Kortatsi (2006). Specific yield values ranged from 2 to 11% and also increased from bottom to top. Based on the decrease in both transmissivity and specific storage in depth, we concluded that the quartzite we encountered in the TSU at 30 m depth was not part of a stratiform fracture layer (SFL) or saprock (e.g. Vassolo et al., 2019). Either the SFL was not present or it must have been below drilling depth. Added to this is the fact that upon drilling the quartzite from 30–50 m, there was no release of pressurized water, which could be the case when reaching the permeable, water containing, SFL. Furthermore, we think the quartzite layer in the TSU at this depth extended up-gradient towards the north, and may even be connected with the quartzite layer in BH1, which could explain the higher groundwater levels in BH8-50 compared to BH8-15. Within the TSU saprolite, roughly east-west oriented, we found a body of conglomerate including subrounded, but also angular fragments. From these observations we concluded that this is a mudflow – alluvial type of deposit, which either indicates the presence or vicinity of the thrust fault between TSU and DSU (as is mentioned in the Introduction) or is related to a higher energy regime of the Dodowa river in the past. From a hydrogeological point of view, the unit is relatively permeable ($T = 3.7e-5$ m²/s).

From the recorded groundwater table fluctuations, which were between 1 and 2 m throughout the year, and assuming unconfined conditions, porosities in the range of 0.5 % for DSU and 5 % for TSU saprolite, while neglecting horizontal flow components, we estimated recharge from precipitation to be in the order of 5–10 mm/year (2–4 % of annual precipitation) for the DSU part of the area and 50–100 mm/year (6–11 % of annual precipitation) for the TSU saprolite part. This is in the same range as, but less than, the 15 % of annual precipitation estimated by Nii Consult (1998) for the Accra Plains, as reported by Kortatsi (2006). Discharge of the spring in October was 20–30 l/s. If we assume this rate is constant for all ~6 wet months per year and if we assume the spring runs dry during the ~6 dry months in any year, then the spring discharges around 0.4 Mm³/year. Based on the groundwater level map, most of the discharge originates from the NW area of the spring, likely from the fractured TSU, as part of the Akwapim-Togo mountains or hills. The boundaries of the catchment area of the spring are unknown, but likely extend to the NW outside the study area as depicted in Fig. 1. Because of the unknown spring catchment boundary, we did not convert nor estimate yearly spring discharge volume to rate of groundwater outflow (mm/day). The (low) concentrations of nitrate we found in the spring water indicated the presence of some waste water or manure pollution, possibly originating from close-by animal farming.

Since groundwater levels did not show any form of overall rise or decline, we assumed the steady-state groundwater balance was square. Besides precipitation excess, other In-terms of the water balance were waste water return and leakage from the water supply mains. Besides spring discharge, other Out-terms of the water balance included abstractions for domestic use, and evapotranspiration, the latter mainly affected groundwater close to the southern part of the study area, where unpolluted brackish NaCl-types of groundwater were found (see below).

Based on the very low ion concentrations from the acid leaching experiments, we conclude that the TSU saprolite was chemically not (very) reactive. Towards the center of the township, we mapped elevated EC, nitrate, and alkalinity, while pH values were lower. Because of the on-site waste water disposal practices of the community, we concluded that on-site infiltration of waste water had occurred. This not only gave rise to elevated concentrations of most ions, but it also explained the relatively high nitrate

Table 2
Measured hydrochemical parameters. Location names are indicated in Fig. 12.

Number	NAME	Type*	UTM E	UTM N	EC µS/cm	pH	Temp. C	Na mmol/L	K mmol/L	Mg mmol/L	Ca mmol/L
1	WAP01	DW	820608	650728	2440	7.3	28.5	16.44	2.07	0.86	1.35
2	WAP02	DW	820604	650681	614	5.8	28.7	2.74	0.74	0.49	0.50
3	WAP03	DW	820604	650540	686	5.4	28.8	3.57	0.82	0.49	0.45
4	WAP04	DW	820644	650529	510	5.5	28.8	2.44	0.43	0.37	0.47
5	WDA05	DW	820420	651059	477	5.6	28.4	2.13	0.38	0.45	0.32
6	WDA06	DW	820406	651024	621	5.6	27.6	2.22	0.41	0.45	0.40
7	WDA07	DW	820465	650783	432	5.2	27.5	2.00	0.28	0.37	0.25
9	WZO 09	DW	820881	650986	1460	5.9	29.5	6.83	1.38	1.44	1.27
10	WYO 10	DW	820687	650797	549	4.7	28	3.00	0.56	0.45	0.27
11	WYO11	DW	820891	650843	3170	6.1	26.9	17.79	0.64	3.21	2.59
12	WYO12	DW	820831	650881	3820	6.3	27	23.36	0.97	3.62	3.87
13	WLO13	DW	820633	651027	602	5.7	28.7	3.61	0.31	0.95	1.00
14	WNU 14	DW	821837	650196	2050	7.5	27.1	11.14	0.18	2.51	3.29
15	BNU 15	BH	821932	650365	2760	7.0	27.3	6.66	0.13	4.81	4.87
16	WNU 16	DW	821893	650468	1535	6.2	27.8	6.48	0.03	2.10	1.97
17	WNU 17	DW	821796	650449	1727	6.3	27.1	6.52	0.13	2.43	2.40
18	WNU 18	DW	821963	650526	740	6.0	27.8	3.18	0.08	0.86	1.00
19	WNU 19	DW	821784	650617	348	5.7	28.2	1.65	0.15	0.16	0.42
21	BWK 21	BH	822538	651087	2650	6.5	28.9	10.83	0.41	4.36	3.27
22	BWK 22	BH	822509	650957	5630	6.4	27.9	30.54	0.20	8.27	5.69
24	WWK 24	DW	822507	651154	1016	6.3	29.3	4.18	0.77	0.70	1.12
25	WHW 25	DW	822363	651420	1744	7.7	29	7.22	1.56	1.36	2.77
27	WRM 27	DW	823156	651414	884	7.0	27.6	2.83	0.49	0.33	2.35
29	BMT 29	BH	822324	651678	2170	6.6	29.3	9.74	0.31	2.84	1.72
30	WMT 30	DW	822291	651636	1632	6.7	29	7.31	2.25	0.91	1.62
34	WNY 34	DW	821357	651409	766	6.5	29.8	3.13	0.59	0.62	1.07
36	WTB 37	DW	821488	651345	1025	5.6	28.3	3.35	0.13	1.36	1.90
37	SWP 38	S	819950	650547	474	6.6	24.5	1.96	0.26	0.37	0.37
39	BH8 – 50 m	BH	821199	650789	753	6.3	29	2.22	0.28	0.99	1.12
40	BH8 – 35 m	BH	821201	650783	1088	6.2	29.8	3.70	0.46	1.56	1.62
41	BH8 – 15 m	BH	821209	650773	946	6.3	29.6	2.52	0.33	1.36	1.50
46	WNU 50	DW	822333	651516	766	6.6	28.6	2.39	0.46	0.66	0.80
47	WOB 53	DW	820099	651404	207	7.8	26	0.52	0.13	0.12	0.20

(continued on next page)

Table 2 (continued)

Number	NH4 mmol/L	Cl mmol/L	HCO3 mmol/L	SO4 mmol/L	NO3 mmol/L	Fe(2) mmol/L	Mn(2) mmol/L	Al mmol/L	Si mmol/L	o.PO4 mmol/L	TOC mmol C/L
1	0.00	11.14	1.65	1.53	3.48	2.0E-04	1.8E-05	1.0E-03	0.50	0.01	0.29
2	0.00	2.26	0.41	0.51	0.90	3.8E-04	5.5E-05	8.6E-03	0.30	0.01	0.07
3	0.00	2.96	0.30	0.58	0.94	2.5E-04	6.7E-04	7.4E-04	0.25	0.00	0.10
4	0.00	2.23	0.30	0.40	0.44	3.9E-04	4.0E-04	4.0E-02	0.28	0.00	0.06
5	0.00	2.20	0.16	0.29	0.65	3.9E-04	1.3E-04	6.8E-02	0.23	0.00	0.15
6	0.00	2.74	0.31	0.45	0.92	2.5E-04	3.6E-05	1.4E-03	0.25	0.00	0.05
7	0.00	2.03	0.22	0.32	0.63	2.8E-03	2.2E-04	8.6E-03	0.22	0.01	0.08
9	0.04	6.40	0.90	0.67	3.60	2.3E-04	3.9E-03	5.9E-03	0.48	0.01	0.12
10	0.00	2.62	0.09	0.55	0.76	6.4E-04	8.6E-04	7.8E-03	0.28	0.01	0.06
11	0.00	16.75	1.93	4.11	0.02	2.3E-04	1.6E-02	3.9E-03	0.37	0.01	0.23
12	0.00	22.99	1.78	5.09	0.85	2.7E-04	2.5E-03	5.2E-04	0.37	0.01	0.30
13	0.00	2.20	0.46	0.83	1.71	2.7E-04	5.5E-04	1.2E-03	0.33	0.01	0.12
14	0.00	14.24	2.29	1.16	0.21	1.4E-04	3.8E-04	1.9E-02	0.52	0.01	0.19
15	0.00	19.52	1.93	0.40	0.00	1.8E-03	2.1E-02	4.8E-03	0.78	0.02	0.10
16	0.00	8.80	1.32	0.75	0.58	2.7E-04	2.6E-03	2.2E-04	0.37	0.00	0.15
17	0.00	10.41	1.35	0.86	1.21	2.9E-04	1.8E-04	3.0E-04	0.42	0.00	0.12
18	0.00	3.78	0.62	0.48	2.90	1.8E-04	5.1E-04	2.2E-04	0.33	0.00	0.18
21	0.00	15.37	2.88	0.05	1.08	3.0E-04	4.0E-04	1.6E-03	0.40	0.00	0.07
22	0.00	43.72	3.98	1.49	0.35	2.0E-03	4.8E-03	7.4E-04	1.03	0.01	0.26
24	0.00	3.84	0.94	2.99	0.13	5.9E-04	9.0E-03	2.2E-04	0.75	0.01	0.19
25	0.00	5.19	2.21	0.98	1.18	2.7E-04	9.1E-05	5.6E-04	0.30	0.01	0.37
27	0.00	1.61	1.19	1.08	4.21	3.0E-04	1.8E-05	5.9E-04	0.40	0.01	0.50
29	0.00	11.99	1.86	0.59	3.06	2.7E-04	5.5E-05	4.5E-03	0.42	0.00	0.26
30	0.00	6.01	1.00	1.10	0.77	0.0E+00	3.6E-05	0.0E+00	1.21	0.03	0.27
34	0.00	2.68	0.68	0.52	3.39	3.4E-04	5.5E-05	5.6E-04	0.27	0.02	0.25
36	0.00	3.30	0.75	0.87	2.69	5.4E-05	1.8E-04	7.7E-03	0.40	0.01	0.15
37	0.00	2.74	2.29	0.15	0.03	0.0E+00	1.1E-04	3.0E-03	0.57	0.01	0.13
39	0.00	2.76	0.79	0.09	1.44	1.4E-03	7.8E-04	2.1E-01	0.27	0.01	0.13
40	0.00	4.51	0.96	0.26	2.39	6.1E-04	5.6E-04	4.0E-02	0.47	0.02	0.10
41	0.00	2.93	1.11	0.36	1.53	9.0E-05	6.6E-04	8.5E-03	0.37	0.01	0.10
46	0.01	3.02	0.64	0.34	0.52	1.5E-03	1.6E-03	6.2E-03	0.30	0.01	0.10
47	0.00	1.13	0.26	0.10	0.00	3.9E-04	3.5E-03	4.1E-02	0.42	0.01	0.32
							1.1E-04	8.9E-04	0.17	0.02	0.32

*: DW = Dug well; BH = drilled well; S = spring.

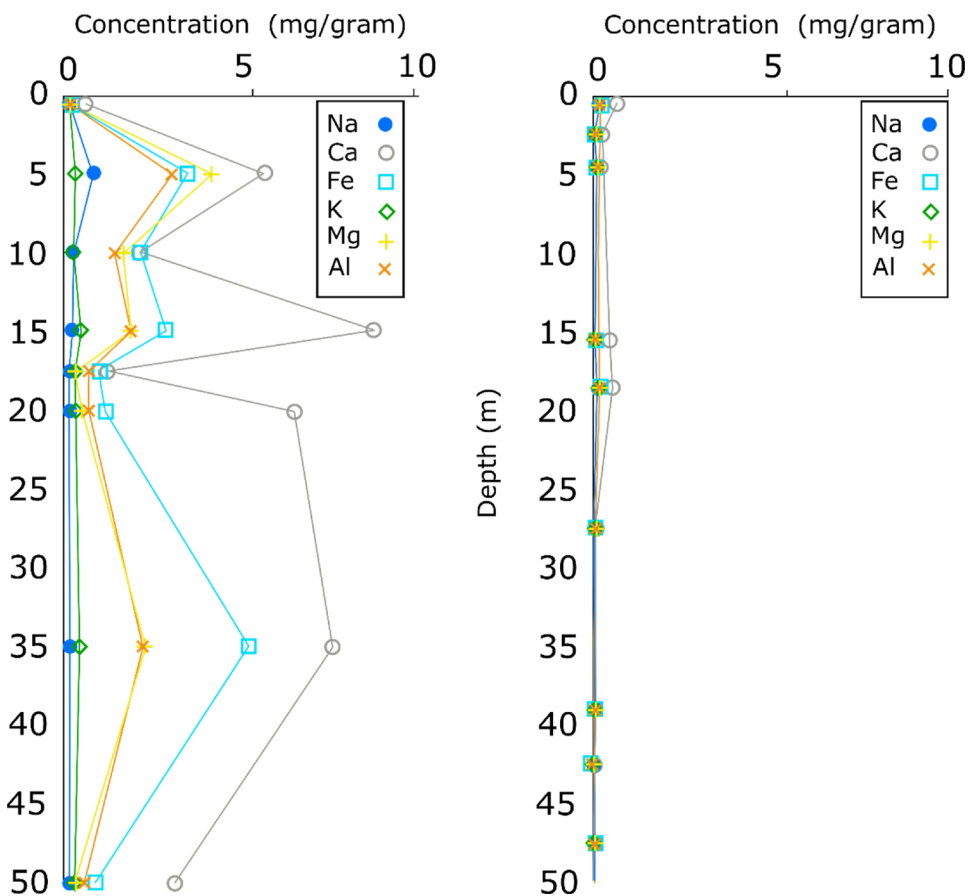


Fig. 11. Ion concentrations as a function of depth for BH11 (left; DSU gneiss) and BH8 (right; TSU saprolite and SFL).

concentrations with here and there traces of ammonium. Assuming that at least some nitrogen in waste water was present as ammonium, apparently, the diffusion of oxygen from the open air into the aquifer was at least equally rapid as the infiltration of waste water in order to maintain aerobic conditions in the upper waste water affected groundwater, whereby ammonium was converted into nitrate, thereby consuming oxygen and producing protons (nitrification). The latter likely caused the pH lowering in this poorly buffered groundwater, although a lower pH compared to natural groundwater pH- values of 7 could also be explained by a slightly acidic pH-value of waste-water. Also, due to the same diffusion of oxygen, since TOC concentrations were in all cases low to very low, mobile TOC originating from the infiltrating waste water, could have decayed, thereby producing CO₂ (and water), which could have added to elevated bicarbonate concentrations. Downstream, the effect of waste water infiltration ceased to exist. Here, in both TSU and DSU, groundwater was composed of unpolluted brackish NaCl-type of water. We think this is the result of evapotranspiration. In absence of the sea (some 30 km away from the study area), weathering of silicate minerals in either TSU saprolite or DSU gneisses produces a NaCl or NaHCO₃ type of water with slightly elevated Ca and Mg concentrations in case of groundwater in the DSU. This water is then evapotranspired, causing brackish groundwater. During the process, minerals will tend to precipitate out of the solution, when the solubility product is exceeded. Kortatsi (2006) suggested halite dissolution to be responsible for the NaCl type of brackish groundwaters. We, however, are more inclined to think that halite is the end product of the evapotranspiration process when all water in solution is evapotranspired.

How to include these findings and insights in a water management plan? In terms of groundwater reserves, based on the present number of wells and measured transmissivities, the TSU saprolite is a reliable source of groundwater, available at very shallow depths. However, given the low volumes of the various terms in the water balance, and the limited volumes stored, any large scale development of groundwater will be difficult or even not possible. Groundwater can only be used in small quantities at a limited scale and preferably not for household use, since the saprolite is rather vulnerable for pollution, as is clear from the confinement determination using tidal analysis and the hydro-chemical data. Groundwater in the DSU can only be obtained from fractures, which are not very frequent, and their transmissivities are very low. Also, groundwater here is mostly brackish, so it is not favorable to develop groundwater sources in DSU in the study area. Due to very thin TSU saprolite towards the south, we expect that groundwater system development in the area is local and confined to the Dodowa area.

From our study, we concluded that:

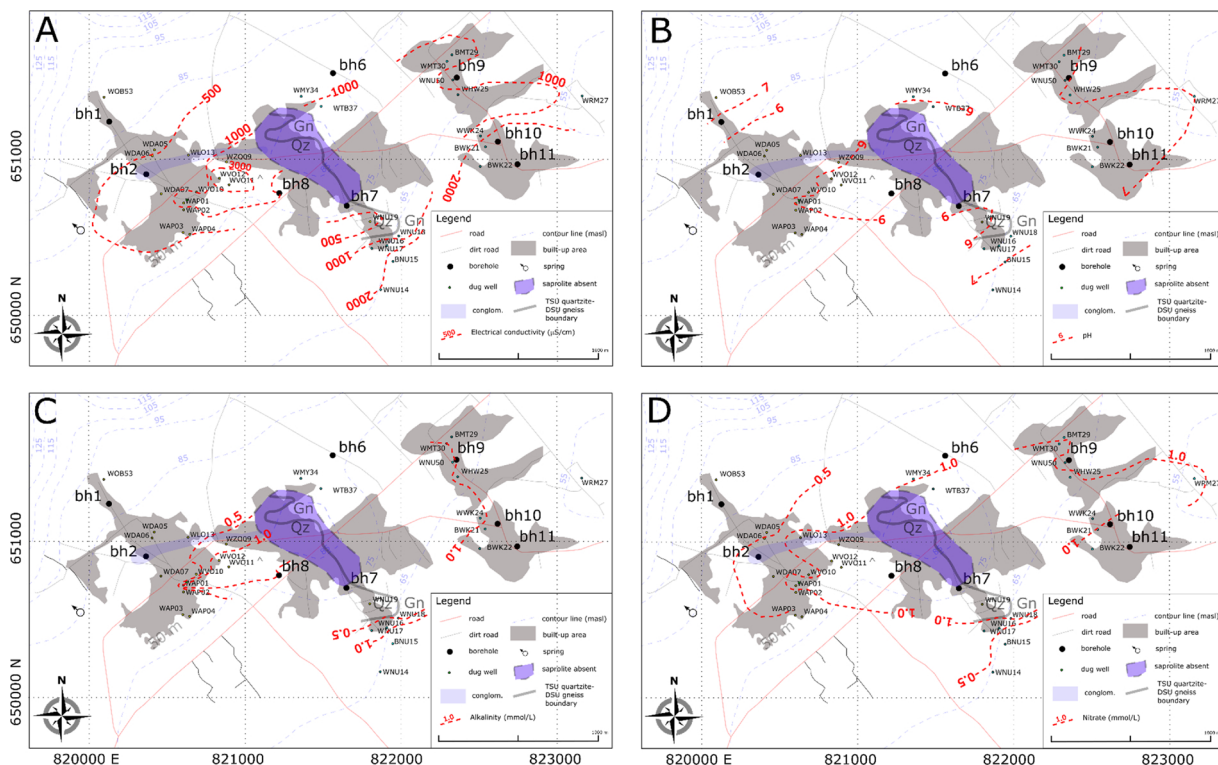


Fig. 12. Contour plots of electrical conductivity (A), pH (B), alkalinity (C), and nitrate (D), measured in dug and drilled wells in the study area.

- Groundwater system dynamics in our study area of only 6 km² was remarkably varied in terms of aquifer thickness, permeability, confinement, groundwater level response to change, and hydrochemistry.
- In the saprolite of the TSU, groundwater occurrence was widespread and at shallow depths. In the DSU, groundwater was found in a limited number of fractures within the parent gneisses. This system was potentially deeper than in case of the TSU.
- Transmissivities of TSU saprolite decreased with depth from 5.4e-5 m²/s at shallow depths to 3.5e-6 m²/s at depths of around 50 m. Specific yield values ranged from 2 to 11%. Transmissivities of the DSU were significantly lower and ranged from 0.2 to 1.2e-6 m²/s.
- The groundwater system was predominantly unconfined. Therefore, the system is vulnerable, evidenced by the widespread on-site infiltration of waste water with elevated EC, alkalinity, and nitrate concentrations, and lower pH-values.
- Downgradient, towards the southern boundary of the study area, the effect of waste water infiltration ceased to exist. Here, groundwater was composed of unpolluted, but brackish, NaCl-type of water.
- Due to very thin saprolite towards the south, we expect that groundwater system development in the area is local and confined to the Dodowa area only.

Declaration of Competing Interest

The authors declare that they have no known competing financial interests or personal relationships that could have appeared to influence the work reported in this paper.

Acknowledgments

The work described above was carried out in the framework of the T-GroUP project. T-GroUP was funded by the UK Department for International Development (DFID), the Economic and Social Research Council (ESRC), and the Natural and Environment Research Council (NERC) under the UPGro Programme, NERC grant number NE/M008045/1. This project has received funding from the European Union’s Horizon 2020 research and innovation programme under the Marie Skłodowska-Curie grant agreement No 835852. We thank the people of Dodowa and the staff of the UNESCO-IHE laboratories for their support.

References

Acworth, R.I., Rau, G.C., McCallum, A.M., et al., 2015. Understanding connected surface-water/groundwater systems using Fourier analysis of daily and sub-daily head fluctuations. *Hydrogeol. J.* 23, 143–159. <https://doi.org/10.1007/s10040-014-1182-5>.

- Acworth, R., Rau, G., Cuthbert, M., Jensen, E., Leggett, K., 2016. Long-term spatio-temporal precipitation variability in arid-zone Australia and implications for groundwater recharge. *Hydrogeol. J.* 24, 905–921.
- Acworth, R.I., Rau, G.C., Halloran, L.J., Timms, W.A., 2017. Vertical groundwater storage properties and changes in confinement determined using hydraulic head response to atmospheric tides. *Water Resour. Res.* 53, 2983–2997. <https://doi.org/10.1002/2016WR020311>Jacob(1940).
- Alle, I.C., Desclouetres, M., Vouillamoz, J.M., Yalo, N., Lawson, F.M.A., Adihou, A.C., 2018. Why 1D electrical resistivity techniques can result in inaccurate siting of boreholes in hard rock aquifers and why electrical resistivity tomography must be preferred: the example of Benin, West Africa. *J. Afr. Earth Sci.* 139 (2018), 341e353. <https://doi.org/10.1016/j.jafrearsci.2017.12.007>.
- Attoh, K., Dallmeyer, R.D., Affaton, P., 1997. Chronology of nappe assembly in the Pan-African Dahomeyide orogen, West Africa: evidence from 40Ar/39Ar mineral ages. *Precambrian Res.* 82 (1–2), 153–171.
- Belle, P., Lachassagne, P., Mathieu, F., Barbet, C., Brisset, N., Gourry, J.-C., 2018. Characterization and location of the laminated layer within hard rock weathering profiles from electrical resistivity tomography: implications for water well siting. In: Ofterdinger, U., Macdonald, A.M., Comte, J.-C., Young, M.E. (Eds.), *Groundwater in Fractured Bedrock Environments*. Geological Society, London. <https://doi.org/10.1144/SP479.7>. Special Publications, 479.
- Carlson, F., Randall, J., 2012. MLU: a windows application for the analysis of aquifer tests and the design of well fields in layered systems. *Ground Water* 50 (4), 504–510. <https://doi.org/10.1111/j.1745-6584.2012.00945.x>.
- Courtois, N., Lachassagne, P., Wyns, R., Blanchin, R., Bougairé, F.D., Somé, S., Tapsoba, A., 2010. Country-scale hydrogeological mapping of hard-rock aquifers and its application to Burkina Faso. *Ground Water* 48, 269–283.
- Dewandel, B., Lachassagne, P., Wyns, R., Maréchal, J.C., Krishnamurthy, N.S., 2006. A generalized 3-D geological and hydrogeological conceptual model of granite aquifers controlled by single or multiphase weathering. *J. Hydrol. (Amst)* 330 (1–2), 260–284. <https://doi.org/10.1016/j.jhydrol.2006.03.026>.
- Edet, A., Okereke, C., 2005. Hydrogeological and hydrochemical character of the regolith aquifer, northern Obudu Plateau, southern Nigeria. *Hydrogeol. J.* 13 (2), 391–415. <https://doi.org/10.1007/s10040-004-0358-9>.
- Foster, S.S.D., 1984. African groundwater development - the challenges for hydrogeological science. *IAHS Publication* 144, 3–12.
- Grönwall, J., 2016. Self-supply and accountability: to govern or not to govern groundwater for the (peri-) urban poor in Accra, Ghana. *Environ. Earth Sci.* 75 (16). <https://doi.org/10.1007/s12665-016-5978-6>. art. no. 1163.
- Guihéneuf, N., Boisson, A., Bour, O., Dewandel, B., Perrin, J., Dausse, A., Viossanges, M., Chandra, S., Ahmed, S., Maréchal, J.C., 2014. Groundwater flows in weathered crystalline rocks: impact of piezometric variations and depth-dependent fracture connectivity. *J. Hydrol. (Amst)* 511, 320–334. <https://doi.org/10.1016/j.jhydrol.2014.01.061>.
- Hemker, C.J., 1999. Transient well flow in vertically heterogeneous aquifers. *J. Hydrol. (Amst)* 225 (1–2), 1–18. [https://doi.org/10.1016/S0022-1694\(99\)00137-7](https://doi.org/10.1016/S0022-1694(99)00137-7).
- Howard, G., Pedley, S., Barrett, M., Nalubega, M., Johal, K., 2003. Risk factors contributing to microbiological contamination of shallow groundwater in Kampala, Uganda. *Water Res.* 37 (14), 3421–3429. [https://doi.org/10.1016/S0043-1354\(03\)00235-5](https://doi.org/10.1016/S0043-1354(03)00235-5).
- Hussein, M.E.A., Odling, N.E., Clark, R.A., 2013. Borehole water level response to barometric pressure as an indicator of aquifer vulnerability. *Water Resour. Res.* 49 (10), 7102–7119. <https://doi.org/10.1002/2013WR014134>.
- Jacob, C.E., 1940. On the flow of water in an elastic artesian aquifer. *Eos, Trans. Am. Geophys. Union* 21, 574–586.
- Kabo-Bah, A.T., Diji, C.J., Nokoe, K., Mulugetta, Y., Obeng-Ofori, D., Akpoti, K., 2016. Multiyear rainfall and temperature trends in the Volta River basin and their potential impact on hydropower generation in Ghana. *Climate* 4 (4). <https://doi.org/10.3390/cli4040049>.
- Kortatsi, B.K., 2006. Hydrochemical characterization of groundwater in the Accra plains of Ghana. *Environ. Geol.* 50 (3), 299–311. <https://doi.org/10.1007/s00254-006-0206-0>.
- Kortatsi, B.K., Jørgensen, N.O., 2001. The origin of high salinity waters in the accra plains groundwaters. In: *Proceedings of the First International Conference on Saltwater Intrusion and Coastal Aquifers - Monitoring, Modeling, and Management*. Essaouira, Morocco, 23–25 April.
- Lachassagne, P., Wyns, R., Dewandel, B., 2011. The fracture permeability of Hard Rock Aquifers is due neither to tectonics, nor to unloading, but to weathering processes. *Terra Nova* 23 (3), 145–161. <https://doi.org/10.1111/j.1365-3121.2011.00998.x>.
- Lapworth, D.J., MacDonald, A.M., Tijani, M.N., Darling, W.G., Goody, D.C., Bonsor, H.C., Araguás-Araguás, L.J., 2013. Residence times of shallow groundwater in West Africa: implications for hydrogeology and resilience to future changes in climate [Temps de séjour de l'eau superficielle en Afrique de l'Ouest: implications hydrogéologiques et résilience aux futurs changements climatiques]. *Hydrogeol. J.* 21 (3), 673–686. <https://doi.org/10.1007/s10040-012-0925-4>.
- Loke, M.H., Barker, R.D., 1996. Practical Techniques for 3D resistivity surveys and data inversion. *Geophys. Prospect* 44, 449–523.
- Lutterodt, van de Vossenbergh, J., Hoiting, Y., Kamara, A.K., Oduro-Kwarteng, S., Foppen, J.W.A., 2018. Microbial groundwater quality status of Hand-Dug Wells and boreholes in the dodowa area of Ghana. *Int. J. Environ. Res. Public Health* 15 (730). <https://doi.org/10.3390/ijerph15040730>.
- MacDonald, A.M., Bonsor, H.C., Dochartaigh, B., Taylor, R.G., 2012. Quantitative maps of groundwater resources in Africa. *Environ. Res. Lett.* 7 (2). <https://doi.org/10.1088/1748-9326/7/2/024009>. art. no. 024009.
- Maréchal, J.C., Wyns, R., Lachassagne, P., Subrahmanyam, K., 2004. Vertical anisotropy of hydraulic conductivity in the fissured layer of hard-rock aquifers due to the geological patterns of weathering profiles. *J. Geol. Soc. India* 63 (5), 545–550.
- McMillan, T.C., Rau, G.C., Timms, W.A., Andersen, M.S., 2019. Utilizing the impact of earth and atmospheric tides on groundwater systems: a review reveals the future potential. *Rev. Geophys.* 57, 281–315. <https://doi.org/10.1029/2018RG000630>Nii. Consult(1998) Information building block. Ghana water management study. Unpublished Consultancy Report for the Ministry of Works and Housing, Ghana, DANIDA, World Bank.
- Parkhurst, D.L., Appelo, C.A.J., 1999. User's Guide to PHREEQC (Version 2)—A Computer Program for Speciation, Batch-Reaction, One-Dimensional Transport, and Inverse Geochemical Calculations. U.S. Geological Survey, Water Resources Investigations Report 99-4259, Washington DC.
- Quist, L.G., 1976. A Preliminary Report on the Groundwater Assessment of the Accra Plains. Unpublished Technical Report. Water Resources Research Institute, C.S.I.R. Ghana.
- Rahi, K.A., Halihan, T., 2013. Identifying aquifer type in fractured rock aquifers using harmonic analysis. *Ground Water* 51, 76–82. <https://doi.org/10.1111/j.1745-6584.2012.00925.x>.
- Rasmussen, T.C., Crawford, L.A., 1997. Identifying and removing barometric pressure effects in confined and unconfined aquifers. *Ground Water* 35 (3), 502–511. <https://doi.org/10.1111/j.1745-6584.1997.tb00111.x>.
- Rau, G.C., 2018. August 17). PyGTide: a Python module and Wrapper for ETERNA PREDICT to Compute Gravitational Tides on Earth (Version v0.2). Zenodo<https://doi.org/10.5281/zenodo.1346664>.
- Rau, G.C., Acworth, R.I., Halloran, L.J.S., Timms, W.A., Cuthbert, M.O., 2018. Quantifying compressible groundwater storage by combining cross-hole seismic surveys and head response to atmospheric tides. *J. Geophys. Res. Earth Surf.* 123 (8), 1910–1930. <https://doi.org/10.1029/2018JF004660>.
- Tsozé, D., Yongue-Fouateu, R., 2017. Tropical chemical weathering of a garnet rich micascist in the rainforest zone of Cameroon. *Eurasian J. Soil Sci.* 6 (1), 1–19. <https://doi.org/10.18393/ejss.284259>.
- Vassolo, S., Neukum, C., Tiberghien, C., Heckmann, M., Hahne, K., Baranyikwa, D., 2019. Hydrogeology of a weathered fractured aquifer system near Gitega, Burundi. *Hydrogeol. J.* 27 (2), 625–637. <https://doi.org/10.1007/s10040-018-1877-0>.
- Wright, E.P., 1992. The hydrogeology of crystalline basement aquifers in Africa. In: In: Wright, E.P., Burgess, W. (Eds.), *Hydrogeology of Crystalline Basement Aquifers in Africa* 66. London Special Publication, pp. 1–27.
- WRRRI, 1996. Groundwater Assessment Report on the Accra Plains. Unpublished Technical Report. Water Resources Research Institute. C.S.I.R., Ghana.
- Wyns, R., Baltassat, J.M., Lachassagne, P., Legchenko, A., Vairon, J., Mathieu, F., 2004. Application of SNMR soundings for groundwater reserves mapping in weathered basement rocks (Brittany, France). *Bulletin de la Société Géologique de France* 175 (1), 21–34.